Research Article

For reprint orders, please contact: reprints@futuremedicine.com

Nanomedicine

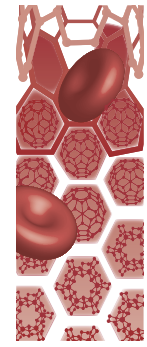

Dual-targeting exosomes for improved drug delivery in breast cancer

Nam HB Tran[‡,1], Diem DN Nguyen[‡,1], Ngoc Mai Nguyen[‡,1], Chau Tran[1], Ngoc Thanh Nguyen Thi[1], Duyen TK Ho[1], Hoai-Nghia Nguyen[1] & Lan N Tu*[,1]

[1]Medical Genetics Institute, Ho Chi Minh City, Vietnam

*Author for correspondence: Tel.: +84 888 843 489; lantu320@gmail.com

[‡]Authors contributed equally

Aims: The authors investigated whether displaying more than one homing peptide enhanced the tumor-targeting efficiency of exosomes. **Materials & methods:** Exosomes from human embryonic kidney cells (HEK293F) were engineered to display either mono- or dual-tumor-penetrating peptides, iRGD and tLyp1. Exosomes were purified via tangential flow filtration followed by ultracentrifugation. **Results:** When loaded with doxorubicin (Dox), the dual iRGD-tLyp1 exosomes strongly enhanced Dox uptake in both MCF-7 and MDA-MB-231 breast cancer cell lines, superior to single iRGD or tLyp1 exosomes. The dual iRGD-tLyp1 exosomal Dox was also the most potent, with IC_{50}/GI_{50} values being 3.7–17.0-times lower than those of free Dox and other exosomal Dox. **Conclusion:** Selecting appropriate combinatorial homing peptides could be an approach for future precision nanomedicine.

First draft submitted: 26 December 2022; Accepted for publication: 30 March 2023; Published online: 17 May 2023

Keywords: breast cancer • doxorubicin • exosomes • gene/drug delivery • iRGD • nanomedicine • tLyp1

Breast cancer (BC) is the most common cancer in humans, with more than 2 million newly diagnosed cases worldwide in 2020 [1]. BC is more prevalent in Asia (45.4%) compared with Europe (23.5%) and North America (12.5%) but universally remains the leading cause of cancer death in women [1]. Chemotherapy, the mainstay of BC treatment for several decades, is recommended as adjuvant therapy for a subset of early-stage BCs and as first-line therapy for a majority of metastatic or recurrent cases. Among many classes of chemotherapy drugs, doxorubicin (Dox) is one of the most potent and effective to slow or stop the growth of cancer cells [2]. However, Dox, similar to other cytotoxic drugs, causes several side effects ranging from mild to severe, acute to long-term problems including pain, fatigue, arrhythmias and even lethal congestive heart failure [2–4]. Such toxicities in nontargeted organs limit the maximum therapeutic doses of these drugs and compromise quality of life for patients. In addition, chemotherapy resistance, particularly multidrug resistance, remains a major dilemma as it often results in therapeutic failure and mortality. Resistance can arise from multiple complex mechanisms, such as reduced drug uptake [5] and strategies to overcome this are limited.

In recent years, nanoparticle drug-delivery systems have emerged as a promising solution to improve targeted delivery and consequently maximize drug dosage, minimize side effects and inhibit resistance. Many researchers have attempted to coat cytotoxic drugs in different forms of nanoparticles, such as H-ferritin-nanocages [6], pH-responsive ZnO quantum dots [7], polymeric nanoparticles, nanoparticle albumin-bound paclitaxel and, most commonly, liposomes [8], such as the Dox-encapsulated liposomes Doxil® and Myocet® that have been US FDA-approved [8,9]. Compared with liposomes, exosomes are one type of extracellular vesicles (EV) released by virtually all mammalian cells, with very similar sizes ranging from 30 to 200 nm [10]. Exosomes participate in cell–cell communication, hence, the composition of their lipid bilayer membrane and endogenous cargo are both far more sophisticated than liposomes. Owing to their biological origin, exosomes have been shown to possess superior biocompatibility, lower immunogenicity and better uptake by recipient cells than liposomes [10].

Another advantage of exosomes is their flexibility for genetic engineering to enhance targeting specificity and uptake efficiency. Several tumor-penetrating and -targeting peptides have been successfully displayed on the surface of exosomes via fusion with exosome surface proteins such as LAMP2B [11] or PDGFR [12]. Internalizing arginine-

Future Medicine

glycine-aspartic acid (iRGD) is the most common tumor-penetrating peptide displayed on exosomes and has been found to effectively target exosomes to BC for Dox delivery [11]. iRGD is a 9-amino-acid cyclic peptide (sequence: CRGDKGPDC) specifically binding to the avβ3 and avβ5 integrins, which are abundantly expressed on tumor vasculatures and tumor cells [13]. Upon binding to avβ3/avβ5 integrins, iRGD exposes the CendR motif that binds to NRP-1, stimulating endocytosis and, hence, cell penetration [13]. Similar to iRGD, truncated Lyp1 (tLyp1) is also a tumor-penetrating peptide but has not been well studied as a homing peptide for exosomes, particularly in BC. Compared with its cyclic parent Lyp1 peptide, the linear tLyp1 (sequence: CGNKRTR) still preserves the 4 amino acid residues (NKRT) responsible for specific binding to the complement C1QBP or p32 receptor [14], a mitochondrial protein expressed as surface receptors on tumor blood vessel endothelial cells and tumor cells in hypoxic or nutrient-deprived regions [15]. The binding of tLyp1 to C1QBP was reported to be weaker than that of Lyp1 but, instead, tLyp1 could directly bind NRP-1 and NRP-2, granting it superior penetrating properties [15].

In this study, the ability of engineered exosomes carrying tumor-homing peptides iRGD and tLyp1 to deliver Dox to BC cells *in vitro* was compared. For the first time, the ability of exosomes with dual tagging of both iRGD and tLyp1 to deliver a cytotoxic drug is reported to be better compared with mono- or non-tagged exosomes.

Materials & methods

Analysis of public genomic datasets

For comparison of gene expression levels, we analyzed the RNA sequencing data of BC patients from The Cancer Genome Atlas (TCGA), Therapeutically Applicable Research to Generate Effective Treatments (TARGET) and Genotype Tissue Expression Project (GTEx) TCGA, that were already combined and normalized [16]. All data were downloaded in transcript-per-million values using the cancer genomics visualization and analysis tool UCSC Xena Brower [17]. The data included the expression levels of examined receptors in normal breast tissue, normal adjacent tissue (NAT), primary breast tumor tissue and distant metastatic sites in either different patients or the same individuals. For survival analysis, microarray data and clinical information were retrieved from 55 independent BC datasets [18]. All datasets had at least 30 patients of all BC subtypes that were not yet systemically treated (total n = 1030 patients). Only the optimal microarray probe sets determined by the JetSet algorithm were used to determine gene expression levels of the receptors [19]. Kaplan–Meier plots were constructed from the expression levels and clinical outcomes of patients using the default settings in the Kaplan–Meier Plotter tool [18].

Cell culture

FreeStyle™ HEK293F cells (Thermo Fisher Scientific, MA, USA) were cultured in CDM4HEK293 medium (Cytiva, MA, USA) supplemented with 1% penicillin–streptomycin and 4 mM L-glutamine (Cytiva). Lenti-X 293T (Takara Bio, Kusatsu, Japan), MDA-MB-231 (ATCC, VA, USA) and MCF-7 (ATCC) cells were cultured in DMEM (Thermo Fisher Scientific) supplemented with 10% (v/v) fetal bovine serum FBS (Cytiva) and 1% penicillin–streptomycin. All cells were maintained in culture flasks at 37°C in a humidified 5% carbon dioxide incubator. Dynamic culture for HEK293F cells was performed in the BioFlo 120 system (Eppendorf, Hamburg, Germany) under the following controlled conditions: temperature at 37°C, pH at 7.2, agitation at 120 r.p.m. and dissolved oxygen at 40%. For each batch, cells were seeded at ~1–2 × 10^5 cells/ml and maintained until the density of ~2 × 10^6 cells/ml was reached.

Lentiviral transduction

Two plasmid constructs consisting of a GNSTM glycosylation motif at the N-terminus followed by either iRGD (CRGDKGPDC) or tLyp1 (CGNKRTR), then human LAMP2B and a HA tag at the C-terminus were cloned in a pLV expression vector as an order from Epoch Life Science (TX, USA). Purified plasmid DNA was transfected into Lenti-X 293T cells using Lenti-X packaging single shots (Takara Bio). Supernatants containing lentiviral particles were harvested 48 h after transfection and used fresh to transduce HEK293F cells at a multiplicity of infection (MOI) = 1 in the presence of 8 μg/ml polybrene (Sigma-Aldrich, MO, USA). After overnight incubation, the medium was replaced with complete CDM4HEK293 medium and cells were maintained for at least 7 days before being evaluated for transgene integration and expression. To generate single iRGD- and tLyp1-expressing cell lines, individual lentiviruses carrying either iRGD or tLyp1 constructs were used to transduce HEK293F cells. To generate the dual iRGD-tLyp1 expressing cell line, the stable iRGD-expressing cells were sequentially transduced with tLyp1 lentivirus. Simultaneous cotransduction of two lentiviruses was not used because it was found to be less effective and unable to obtain a similar integration rate compared with singly transduced cell lines.

Exosome purification

Conditioned media from HEF293F cells were centrifuged at 300 g for 5 min, then at 3000 g for 30 min to remove cells and large debris. Media were then filtered through a 0.2-μm polyethersulfone membrane to remove large EVs. The cleared conditioned media were concentrated using the tangential flow filtration (TFF) system Pellicon® XL 50 (Merck, Darmstadt, Germany) and the Biomax® 300 kDa Membrane (Merck) for 10× concentration. Concentrated media were ultracentrifuged using a 40% sucrose cushion at 120,000 g and 4°C for 3 h. The exosome fraction was washed twice with phosphate-buffered saline (PBS), and the pellet was resuspended in sterile PBS and stored at -80°C. On average, the exosome yield was 3.43 mg/l.

Immunoblotting

Cells and exosomes were lysed in radioimmunoprecipitation assay lysis buffer and the total protein content was determined using the Pierce rapid gold BCA protein assay kit (Thermo Fisher Scientific) according to the manufacturer's instructions. Of the total protein from the lysates, 15–20 μg were separated by SDS-PAGE and then transferred semidry to a nitrocellulose membrane using the Power Blotter system (Thermo Fisher Scientific). The membranes were then blocked with 5% (w/v) bovine serum albumin (BSA) in tris-buffered saline with the addition of 0.1% Tween-20 (TBST) for 1 h before incubation with primary antibodies in the blocking buffer at 4°C overnight. The primary antibodies used were HA (#3724, Cell Signaling, MA, USA), CD81 (#sc-166029, Santa Cruz Biotechnology, CA, USA), CD9 (#ab236630, Abcam, Cambridge, UK), β-actin (#sc-47778, Santa Cruz Biotechnology) and Calnexin (#2679, Cell Signaling). After washing with TBST, the membranes were incubated with goat antimouse IgG secondary antibody (#A32723, Thermo Fisher Scientific) and goat antirabbit IgG secondary antibody (#A21076, Thermo Fisher Scientific) at room temperature for 1 h. Immunoblots were captured with the iBright imaging system (Thermo Fisher Scientific).

Scanning electron microscopy

Purified exosomes were diluted in particle-free PBS. A drop was then deposited on a wafer silicon surface, dried and coated with platinum metals. Scanning electron micrographs of exosomes were obtained with a Hitachi S-4800 FESEM (Hitachi High-Technologies, Tokyo, Japan).

Particle concentration & size measurement

Samples were diluted in particle-free PBS and clarified immediately prior to use with a 0.2-μm filter to minimize the presence of nanometer-scale phosphate crystals. Particle concentration and size distribution were measured using a ZetaSizer Ultra machine (Malvern Panalytical, Malvern, UK).

Exosome labeling with PKH67

A PKH67 green fluorescent cell linker kit (Sigma-Aldrich) was used for exosome labeling following the manufacturer's instructions. Briefly, 6×10^9 exosomes and 8 μM PKH67 dye were separately diluted in the diluent C of the kit and then mixed together at a 1:1 volume ratio. After 5 min incubation at room temperature, 1% BSA was added and incubated for 1 min to stop the staining. The mixture was then diluted in PBS and labeled exosomes were recovered via ultracentrifugation with 40% sucrose cushion at 120,000 g for 18 h at 4°C. The exosome pellet was further washed with PBS and freshly labeled exosomes were used immediately for exosome uptake assays.

Exosome loading with Dox

Dox (Tocris Bioscience, Bristol, UK) was diluted in ultrapure water to make a stock of 10 mM. Subsequent dilutions of the 10 mM stock were carried out using PBS. Purified exosomes were incubated with Dox at various concentration ratios for 4 h at 25°C. In one set of experiments, Dox was loaded on exosomes by electroporation in three conditions: 500 V, 10 pulses and 20 ms; 750 V, 10 pulses and 20 ms; 1000 V, 2 pulses and 10 ms, using the Neon™ transfection system (Thermo Fisher Scientific). The Exo-Dox mixture was washed twice with PBS using 30 kDa MWCO Pierce protein concentrators (Thermo Fisher Scientific) to remove excess Dox. Loaded Dox was quantified against a standard curve starting at 20 ng/μl using the Nano F Plus (Tecan, Switzerland; excitation = 485 nm ± 20 nm; emission = 535 nm ± 25 nm). The loading efficiency was calculated as the average percentage of the loaded drug (ng) over the total drug input (ng). Freshly loaded exosomes were used immediately for exosome uptake and MTT cell viability assays.

Exosome uptake assays

For PKH67-labeled exosomes, 100,000 cells were seeded on each well in a 12-well plate for both MCF-7 and MDA-231 cells; 1×10^9 and 5×10^7 exosomes were incubated with the cells for 4 h and 18 h, respectively. For Dox-loaded exosomes, MCF-7 and MDA-231 cells were seeded at a density of 48,000 cells/well and 60,000 cells/well, respectively, on a 24-well plate. Cells were then treated with 0.3 ng/µl free Dox and different Exo-Dox samples for 2 h. After incubation, cells were washed once with PBS and used for fluorescence imaging using the EVOS M5000 imaging system (Thermo Fisher Scientific) and for flow cytometry using the BD Accuri C6 Plus flow cytometer (BD Bioscience, NJ, USA; FITC channel for PKH67 and PE channel for Dox). Flow cytometry data were analyzed using FlowJo v10 software (BD Life Science, NJ, USA).

MTT cell viability assay

On a 96-well plate, MCF-7 cells were seeded at 7000 cells/well and MDA-231 cells were seeded at 15,000 cells/well. Cells were treated with 8 points of twofold diluted free Dox or Exo-Dox, with the highest concentrations being 1.2 ng/µl and 6 ng/µl for MCF-7 and MDA-231 cells, respectively. A CyQUANT MTT cell proliferation assay kit (Invitrogen, CA, USA) was used according to the manufacturer's instructions. Briefly, 10 µl of 12 mM MTT was added to wells containing fresh medium and incubated for 3 h at 5% CO_2 and 37°C. All but 25 ul of medium was carefully removed and 100 µl DMSO was added and incubated for 10 min at 37°C to dissolve the insoluble formazan. All wells were gently resuspended to mix and the absorbance was read at 492 nm using the Nano F Plus (Tecan, Zürich, Switzerland).

Statistical analysis

For analysis of gene expression data, Kruskal–Wallis analysis with *posthoc* Dunn's test was performed to compare expression levels among different groups of tissues. The Wilcoxon test was used to compare the expression ratio of tumor/NAT with a value of 1. Survival curves were analyzed by the Kaplan–Meier method and log-rank test. For all *in vitro* assays, one-way analysis of variance with *post hoc* Bonferroni's multiple comparison tests was used. IC_{50} and GI_{50} values for Dox were obtained in GraphPad Prism by plotting the concentration of Dox in log scale and percentage of viability; curve fitting was done using a four-parameter logistic equation. All statistical tests were performed using GraphPad Prism. Bar graphs indicated mean ± standard error of the mean; $p < 0.05$ was considered significant.

Results

Overexpression of receptors for iRGD & tLyp1 in BC

The expression levels of receptors that are potentially enriched on the membrane of tumor blood vessel endothelial cells and tumor cells in BC were investigated. Receptors for the tumor-penetrating peptides iRGD and tLyp1 include αvβ3/5, C1QBP and NRP-1/2 (Figure 1A). Using large gene expression datasets, expression levels of these receptors were compared in four independent cohorts of breast tissues: normal breast, NAT of the tumor, primary breast tumor and distant metastatic sites. The results showed significant upregulation of *C1QBP*, *ITGAV* and *ITGB5* in breast tumors compared with normal or NAT tissues (Figure 1B & Supplementary Figure 1A). *C1QBP* was the only gene significantly upregulated in the metastatic sites compared with normal breast tissue (Figure 1B). The expression levels between paired NAT and breast tumors in the same individual patients were then examined. The expression ratios of tumor/NAT for *C1QBP*, *ITGAV* and *ITGB5* genes were significantly higher than 1 (Figure 1C). Kaplan–Meier plots were constructed to identify the association of gene expression levels with overall survival and relapse-free survival of BC patients. High expression of *C1QBP* was significantly associated with poor prognosis in BC (Figure 1D) while other receptors did not show any association (Supplementary Figure 1B).

Engineering & purification of exosomes carrying single- & dual-homing peptides

Two plasmid constructs fusing either iRGD or tLyp1 to the exosome membrane protein LAMP2B were used for display (Figure 2A). The GNSTM glycosylation motif was used at the N-terminus to protect the display peptides from proteolytic degradation [20]. Lentiviruses carrying these constructs were produced from LentiX-293T cells. HEK293F cells were then transduced with one or two lentiviruses sequentially to generate stable cell lines. Control wild-type (WT) cells were not transduced. There were four types of cells corresponding to four types of exosomes: WT, iRGD, tLyp1 and dual peptides (Figure 2A).

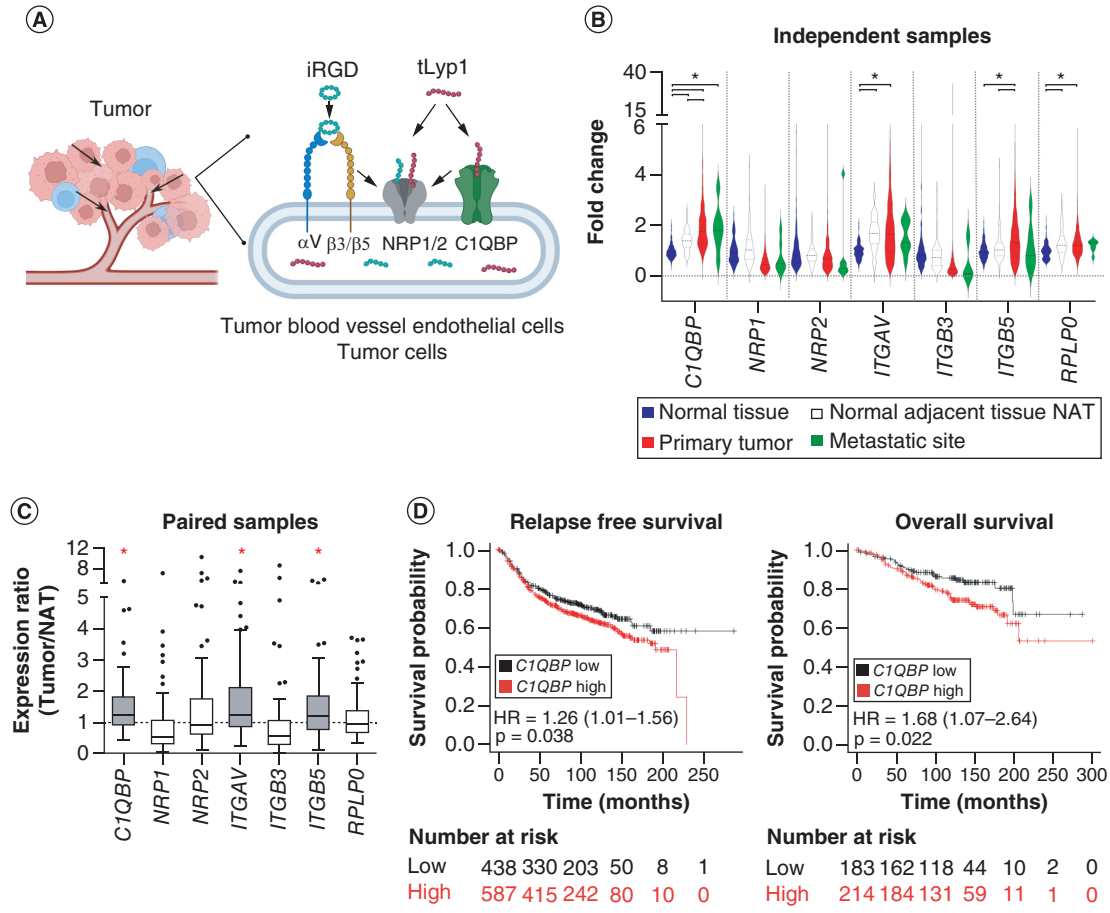

Figure 1. Expression of receptors for tumor-penetrating peptides iRGD and tLyp1 in breast cancer. (A) Tumor microenvironment: tumor blood vessel endothelial cells and tumor cells (arrows) expressed receptors αvβ3, αvβ5, NRP-1, NRP-2 and C1QBP. iRGD first binds αvβ3/5, gets cleaved and exposes its CendR motif that binds to NRP-1 for internalization. tLyp1 binds C1QBP and NRP-1/2 directly. **(B)** Gene expression levels were retrieved from combined TCGA-TARGET-GTEx databases for four independent sets of breast tissues: normal breast, NAT, primary breast tumor and distant metastatic site. Violin plot compares gene expression levels of *C1QBP*, *NRP1*, *NRP2*, *ITGAV*, *ITGB3*, *ITGB5* and *RPLP0* among the four sets (normal = 179, NAT = 113, tumor = 1092, metastatic site = 7). *RPLP0* was used as a reference gene. **(C)** Gene expression levels for paired NAT and primary breast tumors in the same patients were compared (n = 112). The expression ratio of tumor/NAT was significantly higher than 1 for *C1QBP*, *ITGAV* and *ITGB5* genes. **(D)** Kaplan–Meier plots showed that a high level of *C1QBP* was significantly associated with shorter relapse-free survival and overall survival. *$p < 0.05$.
NAT: Normal adjacent tissue.

HEK293F suspension cells were cultured in chemically defined media CDM4HEK293F in a bioreactor for exosome production. Conditioned media was first subjected to differential centrifugation and 0.2-μm filtration to remove cells, debris and large EVs, followed by TFF with 300 kDa membrane for 10× concentration. Media was then ultracentrifuged with 40% sucrose cushion and the purified pellets were resuspended in sterile particle-free PBS for storage at -80°C (Figure 2B). In all subsequent experiments, two BC cell lines, MCF-7 and MDA-MB-231 (or MDA-231), were used to evaluate the therapeutic effectiveness of the engineered exosomes. The expressions of two major receptors (αvβ3 and C1QBP) for iRGD and tLyp1, respectively, were quantified by flow cytometry. The result showed that MCF-7 cells expressed both of these surface receptors more than MDA-231 cells (Figure 2C).

Characterization of engineered cells & exosomes

Total mRNA was extracted from engineered HEK293F cells and amplified using primers binding specifically to the exogenous iRGD and tLyp1 sequences. Gel electrophoresis showed clear bands of mRNA expression of the correct peptide(s) in the iRGD, tLyp1 and dual iRGD-tLyp1 cells (Figure 3A). Western blot analysis

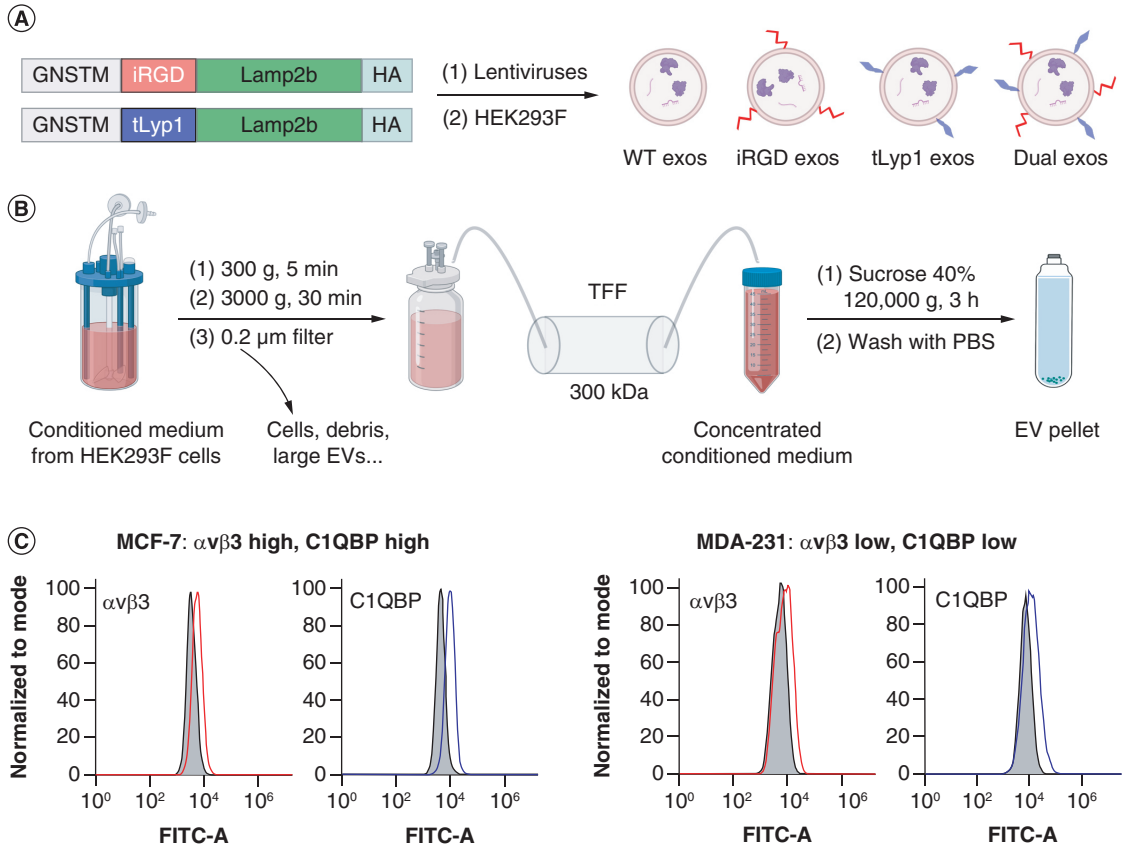

Figure 2. Design and workflow of the study. (A) Plasmid constructs used to display iRGD and tLyp1 on the surface of exosomes included GNSTM glycosylation motif, homing peptide(s) fused with LAMP2B and HA tag at the C-terminus. Lentiviruses carrying these constructs were produced in LentiX-293T cells. HEK293F were then transduced with single iRGD/tLyp1 lentiviruses, or consecutively with both lentiviruses to generate stable cell lines. Exosomes from these lines were divided into four groups: WT, iRGD, tLyp1 and dual iRGD-tLyp1. **(B)** Workflow of exosome isolation and purification. Conditioned media from HEK293F cells was subjected to differential centrifugation and TFF followed by ultracentrifugation with 40% sucrose cushion. **(C)** Purified exosomes were treated on two breast cancer cell lines MCF-7 and MDA-MB-231 (MDA-231). Flow cytometry analysis of surface αvβ3 and C1QBP showed that MCF-7 cells expressed both surface receptors more than MDA-231 cells.
EV: Extracellular vesicle; TTF: Tangential flow filtration; WT: Wild-type.

demonstrated expressions of the exogenous HA-tagged iRGD-LAMP2B and tLyp1-LAMP2B proteins in the corresponding cell lysates and exosome lysates (Figure 3B), confirming the successful generation of four types of exosomes. Size distribution analysis showed the average size of WT exosomes to be 123.10 nm and the engineered exosomes were slightly larger: 145.50 nm, 147.50 nm and 134.50 nm for the iRGD, tLyp1 and dual iRGD-tLyp1 exosomes, respectively (Figure 3C). The morphology of the purified WT exosomes was assessed by scanning electron microscopy (SEM), displaying mostly individual round and intact exosomes (Figure 3D). There was no difference in the SEM images among different types of exosomes (data not shown).

Dual iRGD-tLyp1 exosomes increased cellular uptake & drug delivery

MCF-7 and MDA-231 cells were incubated with PKH67-labeled exosomes for 4 h and 18 h. Cellular uptake was assessed by the percentage of cells positive for PKH67 fluorescent signal. After 4 h of incubation with dual iRGD-tLyp1 exosomes, there was a modest increase (~11%) in cellular uptake in MCF-7 cells compared with WT exosomes (Figure 4A & B). The number of exosomes being internalized was then quantified by the median fluorescent intensity of the PKH67 signal in cells. At 18 h after incubation, although all the cells were positive for PKH67 (Figure 4A), MCF-7 cells internalized significantly more engineered exosomes than WT exosomes (Figure 4C). In MDA-231 cells, the difference was more pronounced in that dual iRGD-tLyp1 exosomes were endocytosed significantly more than the single iRGD and tLyp1 exosomes, and ~41% more than WT exosomes

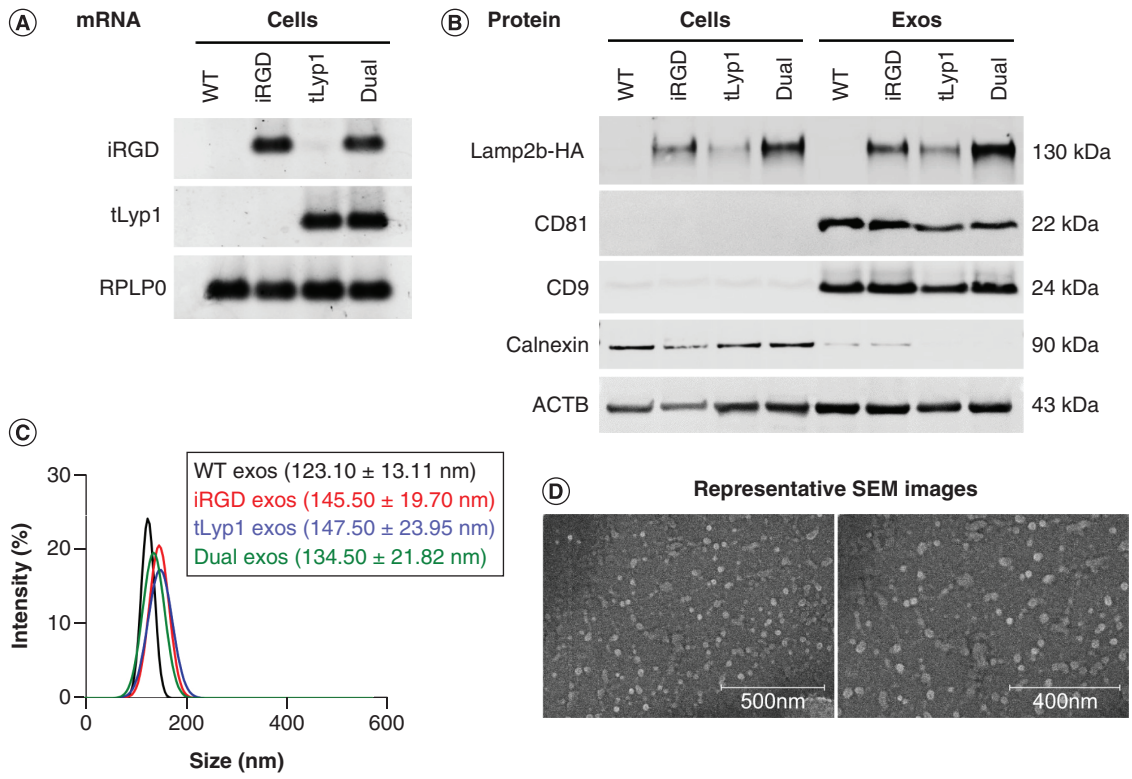

Figure 3. Characterization of engineered HEK293F cells and exosomes. (A) mRNA expressions of exogenous iRGD and tLyp1 constructs in engineered HEK293F cells. There was no amplification of both sequences in WT cells. **(B)** Immunoblots confirmed protein expressions of iRGD- and tLyp1-LAMP2B-HA in both cells and exosomes. CD81 and CD9 were positive markers for exosomes while Calnexin was a negative marker. **(C)** Size distribution of wild type and engineered exosomes. **(D)** Representative SEM showing intact purified exosomes.
SEM: Scanning electron micrograph; WT: Wild-type.

(Figure 4C & D). There were no morphological changes or cell death in both cell lines after incubation with four types of exosomes (Figure 4D).

Exosomes were next loaded with the cytotoxic drug Dox via different methods: incubation or electroporation at 500 V, 10 pulses; 750 V, 10 pulses and 1000 V, 2 pulses using the Neon transfection system. The efficiency of Dox loading as well as exosome recovery were found highest in the incubation method (Supplementary Figure 2A), which was therefore chosen for downstream experiments. The accuracy of Dox-loading quantification was verified using three sets of samples: exosome only, free Dox only and exosomes incubated with Dox. After washing, only the sample with both exosomes and Dox had a high fluorescence signal, corresponding to the Dox loaded into exosomes (Supplementary Figure 2B). The average exosome recovery rate was 53.70% after Dox loading and washing steps as shown by a representative immunoblot (Supplementary Figure 2C). The input ratio of Dox to exosome was carefully assessed to achieve the best loading efficiency. Using a ratio of 1×, which was equivalent to 1 μM Dox per 2 × 10^8 exosome particles, a loading efficiency of only ~10.75% was obtained. Increasing the ratio to 16× yielded an average reproducible loading efficiency of ~22.75%, which was then used for subsequent loading experiments (Supplementary Figure 2D). The addition of triethylamine did not improve the amount of loaded Dox (Supplementary Figure 2E). The drug-loading efficiency and exosome recovery rate are compared with previous studies in Supplementary Table 1. The size distribution of exosomes after Dox loading was wider than that of exosomes before loading but the mean size was not different (Supplementary Figure 2F & G).

After optimization, Dox was loaded on four types of exosomes. The loading efficiency and exosome recovery were fairly consistent among the four groups of exosomes (Supplementary Figure 3A & B). MCF-7 and MDA-231 cells were treated with the Dox-loaded exosomes or with free Dox for comparison. For Dox uptake assessment, flow cytometry was performed after 2 h of treatment. The results revealed a substantial increase in both the percentage of positive cells and median fluorescent intensity of Dox when the cells were treated with dual Exo-Dox compared

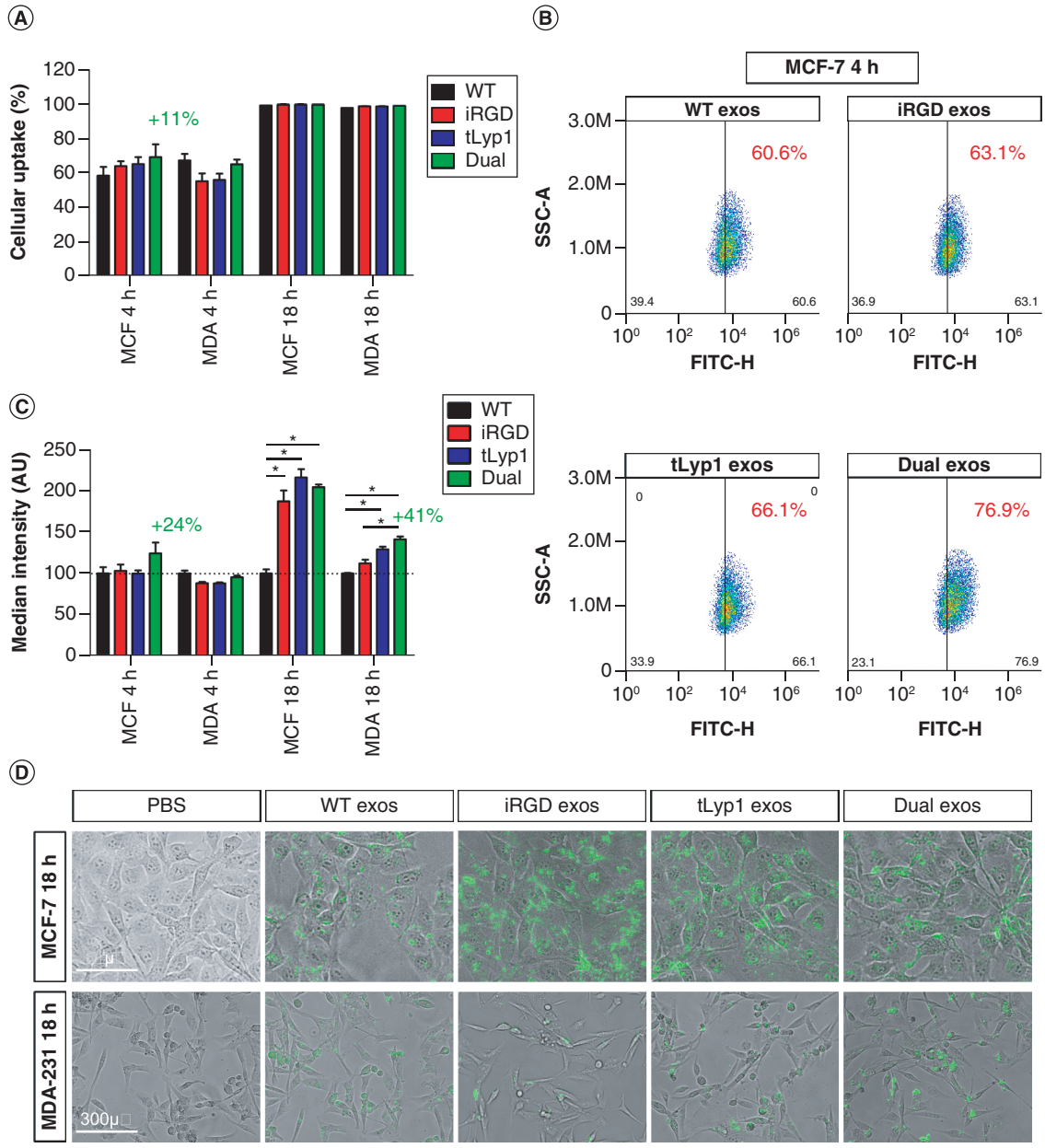

Figure 4. Internalization of exosomes labeled with PKH67 in MCF-7 and MDA-231 cells. (A & B) Cellular uptake of labeled exosomes was analyzed by flow cytometry. At 4 h after treatment, percentage of PKH67-positive MCF-7 cells in dual iRGD-tLyp1 exosome-treated group was ~11% higher than wild-type exosome-treated group. **(C)** Median fluorescent intensity of cells treated with labeled exosomes was analyzed by flow cytometry. At 18 h after treatment, intensity was significantly higher in all engineered exosome-treated groups compared with wild-type group. **(D)** Representative fluorescence images of MCF-7 and MDA-231 cells showing higher uptake of engineered exosomes by MCF-7 cells compared with wild-type exosomes; while MDA-231 images showed greatest fluorescence signal in cells treated with dual exosomes compared with other groups.
n = 3; *p < 0.05.
PBS: Phosphate-buffered saline; WT: Wild-type.

with the WT or single iRGD and tLyp1 Exo-Dox alone (Figure 5A & B). Representative fluorescence images of MCF-7 and MDA-231 cells also showed brighter Dox signals in cells treated with dual Exo-Dox (Supplementary Figure 3C). These cell lines were next treated with a range of free Dox and Exo-Dox for 48 h to assess the relative IC_{50} and absolute concentration that inhibits cell growth by 50% (GI_{50}). The calculation metrics are different for these values as GI_{50} assumes a range of 0–100% viability while IC_{50} uses experimental data for a min-to-max

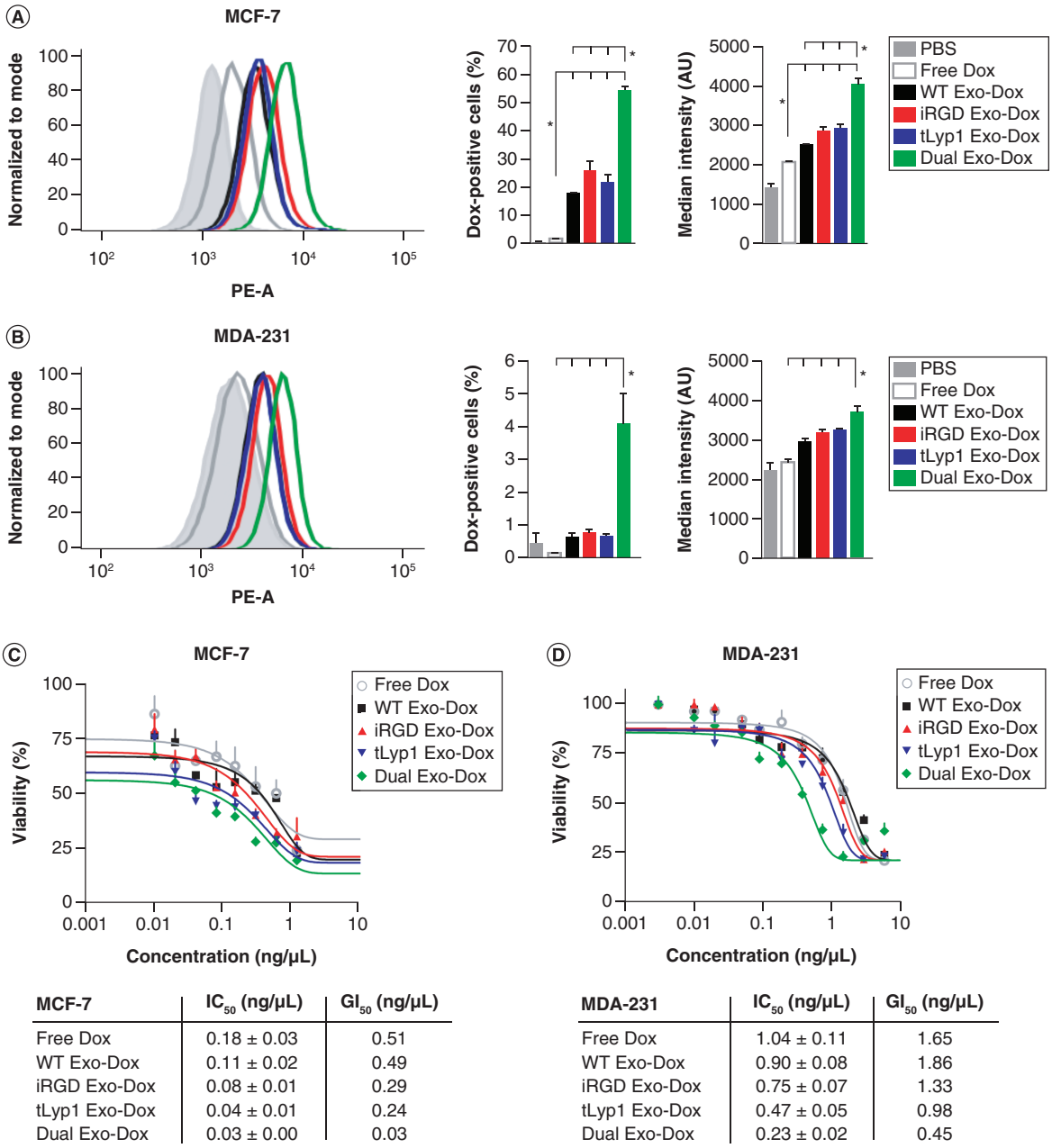

MCF-7	IC_{50} (ng/μL)	GI_{50} (ng/μL)
Free Dox	0.18 ± 0.03	0.51
WT Exo-Dox	0.11 ± 0.02	0.49
iRGD Exo-Dox	0.08 ± 0.01	0.29
tLyp1 Exo-Dox	0.04 ± 0.01	0.24
Dual Exo-Dox	0.03 ± 0.00	0.03

MDA-231	IC_{50} (ng/μL)	GI_{50} (ng/μL)
Free Dox	1.04 ± 0.11	1.65
WT Exo-Dox	0.90 ± 0.08	1.86
iRGD Exo-Dox	0.75 ± 0.07	1.33
tLyp1 Exo-Dox	0.47 ± 0.05	0.98
Dual Exo-Dox	0.23 ± 0.02	0.45

Figure 5. Cellular uptake and IC_{50} of doxorubicin-loaded exosomes in MCF-7 and MDA-231 cells. (A) MCF-7 and **(B)** MDA-231 cells were treated with 0.3 ng/μl free Dox, wild type, iRGD, tLyp1 or dual Exo-Dox for 2 h and analyzed via flow cytometry for Dox fluorescence signal. In both cell lines, Dox uptake was highest in cells treated with dual Exo-Dox. **(C)** MCF-7 and **(D)** MDA-231 cells were treated with a range of free Dox, wild type, iRGD, tLyp1 or dual Exo-Dox for 48 h to determine their IC_{50} and GI_{50} values. Among all treatments, IC_{50} and GI_{50} values of dual Exo-Dox were lowest in both cell lines. n = 3, *$p < 0.05$.
Dox: Doxorubicin; Exo-Dox: Exosomal doxorubicin; GI_{50}: Concentration for 50% growth inhibition; PBS: Phosphate-buffered saline; WT: Wild-type.

percentage of viability. In both cell lines, free Dox showed the highest IC_{50} and GI_{50} values, followed by the WT Exo-Dox, iRGD Exo-Dox, tLyp1 Exo-Dox and dual Exo-Dox. In MCF-7 cells, IC_{50} of dual Exo-Dox was 6-times lower than that of free Dox and 3.7-times lower than that of WT Exo-Dox (Figure 5C). In MDA-231 cells, IC_{50} of dual Exo-Dox was 4.5- and 3.9-times lower than that of free Dox and WT control, respectively (Figure 5D). The difference in GI_{50} values was more remarkable, in that the GI_{50} of dual Exo-Dox was 3.7–17.0-times lower than those of other groups. Overall, dual Exo-Dox was found the most potent among all types of Dox. The cellular

uptake and therapeutic effectiveness of the Exo-Dox were compared with previous nanosystems in Supplementary Tables 2 & 3. There was no cell death observed from both cancer cell lines after 48 h incubation with exosomes alone (Supplementary Figure 3D).

Discussion

In this study, we examined the ability of engineered exosomes carrying tumor-penetrating peptides iRGD and tLyp1 to deliver Dox to BC cells *in vitro.* The receptors for these peptides have been examined in previous studies using semiquantitative immunohistochemistry with limited sample numbers. Both integrins and *C1QBP* were reported to be overexpressed in breast tumor tissues [21–23], and expression of *C1QBP*, not integrins, could be a prognostic factor for survival [21–23]. Our approach utilized next-generation sequencing data obtained from large-sample, multiethnic and multinational cohorts to re-evaluate the relevance of these receptors in BC. The results agreed with previous reports that *C1QBP*, *ITGAV* and *ITGB5* were upregulated in breast tumors compared with not only normal breast but also the NAT in the same patients. Of all receptors, *C1QBP* was the only gene associated with survival, making it a viable targeting candidate for drug delivery. Despite the rapid growth of exosome research, displaying tLyp1 on the surface of exosomes has been limited to only one *in vitro* study in lung cancer [24]. Exploring the combination of more than one tumor-penetrating peptide for potential synergistic advantages is also lacking.

We chose HEK293F cells as the exosome production cells as they are of noncancer origin, easy to genetically manipulate and exosomes derived from HEK293F cells have been extensively characterized to be safe both *in vitro* and *in vivo* [25,26]. The plasmid constructs used LAMP2B with the glycosylation motif GNSTM to stabilize the display peptides without affecting their binding to the receptors [20]. After a series of differential centrifugation, TFF and ultracentrifugation, the exosomes appeared intact and the engineered exosomes were 10–15% larger than WT exosomes. Such a modest increase in size has been reported in engineered exosomes [27,28] but the exact mechanism and functional impact are not understood.

Drug loading into exosomes can be a passive (i.e., via incubation), active (i.e., via electroporation, sonication, extrusion, freeze–thaw) or combined process. In previous studies, the loading efficiency, measured as the percentage of the loaded drug over the total drug input, ranged 4–32% and the exosome recovery rate was 20–50% by these methods [29–33]. In this study, we optimized the loading process using both incubation and various electroporation protocols and concluded that for Dox loading, incubation was more efficient with an average loading efficiency of 22.75% and exosome recovery of 53.70%, comparable with the literature [29–33].

For exosome uptake assays, overall, we observed more active uptake in MCF-7 than MDA-231 cells for both PKH67-labeled and Dox-loaded exosomes. This was likely attributed to the higher expressions of integrins and *C1QBP* in our MCF-7 cell line. The uptake assay of PKH67-labeled exosomes suggested a modest advantage of the dual iRGD-tLyp1 exosomes over the other groups but the difference was not dramatic, probably due to the saturation of fluorescent signals, especially in MCF-7 cells. We also did not observe significantly more uptake in PKH67-labeled iRGD exosomes than WT exosomes at 4 h after incubation as demonstrated in earlier reports [11,27]. This could be due to the different doses of exosomes and cell lines we used for treatment. In the analysis of Dox-loaded exosomes, the impact of engineering was much more pronounced. There was a strong increase in the amount of Dox delivered into both cell lines by the dual iRGD-tLyp1 exosomes compared with the single iRGD, tLyp1 or WT exosomes, resulting in a 3.7–17.0-fold reduction in the IC_{50} and GI_{50} values for dual-exosomal Dox. The Dox-loading efficiency and exosome recovery rate after loading were thoroughly controlled and showed no difference among experimental groups, indicating that the observation was genuine. The relative IC_{50} is influenced by the minimum and maximum viability (%) in curve fitting, and our data did not include two concentrations below the lower bend point, hence, GI_{50} is probably a more reliable measure for cytotoxicity in this experiment [34]. Compared with previous studies, Exo-Dox has been reported to be more potent than free Dox but at varying degrees, from insignificant to 1.6–20-fold, which could be attributed to different cell line models and cell viability assays [29,32,35]. Our WT Exo-Dox was found 1.2-fold and 1.6-fold more potent than free Dox in MDA-231 and MCF-7 cells, respectively. The single iRGD Exo-Dox further reduced IC_{50}/GI_{50} by 20–40% compared with WT Exo-Dox, and tLyp1 Exo-Dox seemed to be more effective than iRGD Exo-Dox. The superior potency of dual iRGD-tLyp1 Exo-Dox was not additive of the single Exo-Dox as the GI_{50} of iRGD and tLyp1 exosomal Dox were more than two-fold the GI_{50} of dual exosomal Dox. Therefore, we speculate that displaying both homing peptides on the exosomes yielded a synergistic effect to increase cellular penetration and, hence, Dox potency. This system would allow the use of a lower Dox concentration to achieve a similar therapeutic effect and reduced side effects compared with free Dox.

Conclusion

For the first time, the ability of exosomes displaying dual tumor-penetrating peptides iRGD and tLyp1 for Dox delivery was examined. The results showed better uptake by recipient cells and higher potency of dual iRGD-tLyp1 Exo-Dox compared with free Dox or other single Exo-Dox. This improvement in targeted delivery has great potential to increase the therapeutic index for cytotoxic drugs used in the management of both primary BC and chemotherapy-resistant cases. Such nano-delivery systems could also help accelerate drug discovery, particularly for candidates with adequate efficacy but poor toxicity profiles. Finally, although the data must still be validated *in vivo*, this strategy of combining multiple homing peptides could be further explored to maximize the targeting efficiency of exosomes for different types of cancers and empower precision nanomedicine in the future.

Summary points

- Engineered exosomes are emerging as promising drug carriers to specifically target cytotoxic drugs to tumors and hence improve drug efficacy and safety.
- In breast cancer, exosomes displaying a combination of more than one homing peptide have not been investigated.
- In this study, exosomes were engineered from human embryonic kidney cells (HEK293F) to display either mono- or dual-tumor-penetrating peptides iRGD and tLyp1 on the surface.
- When labeled with PKH67 dye, the dual iRGD-tLyp1 exosomes showed a significant increase in cellular uptake in MDA-MB-231 cells compared with other groups.
- Incubation was found to be the best method to load doxorubicin (Dox) to exosomes.
- Dox-loading efficiency was 22.8% and the exosome recovery rate was 53.7%.
- When loaded with Dox, the dual iRGD-tLyp1 exosomes strongly enhanced Dox uptake in both MDA-MB-231 and MCF-7 cells, superior to the single iRGD or tLyp1 exosomes.
- Dual iRGD-tLyp1 exosomal Dox was the most potent with the lowest IC_{50}/GI_{50} values that were 3.7–17.0-times lower than those of free Dox and other exosomal Dox.
- These engineered exosomes carrying two tumor-homing peptides have potential advantages to improve exosome-based drug delivery.

Supplementary data

To view the supplementary data that accompany this paper please visit the journal website at: www.futuremedicine.com/doi/suppl/10.2217/nnm-2022-0328

Financial & competing interests disclosure

This study was funded by NexCalibur Therapeutics, Corp. The funder did not have any role in the study design, data collection and analysis or preparation of the manuscript. The authors have no other relevant affiliations or financial involvement with any organization or entity with a financial interest in or financial conflict with the subject matter or materials discussed in the manuscript apart from those disclosed.

No writing assistance was utilized in the production of this manuscript.

References

Papers of special note have been highlighted as: • of interest

1. Sung H, Ferlay J, Siegel RL *et al.* Global cancer statistics 2020: GLOBOCAN estimates of incidence and mortality worldwide for 36 cancers in 185 countries. *CA Cancer J. Clin.* 71(3), 209–249 (2021).
2. Carvalho C, Santos RX, Cardoso S *et al.* Doxorubicin: the good, the bad and the ugly effect. *Curr. Med. Chem.* 16(25), 3267–3285 (2009).
3. Saibil S, Fitzgerald B, Freedman OC *et al.* Incidence of taxane-induced pain and distress in patients receiving chemotherapy for early-stage breast cancer: a retrospective, outcomes-based survey. *Curr. Oncol.* 17(4), 42–47 (2010).
4. Swain SM, Whaley FS, Ewer MS. Congestive heart failure in patients treated with doxorubicin: a retrospective analysis of three trials. *Cancer* 97(11), 2869–2879 (2003).

5. Mansoori B, Mohammadi A, Davudian S, Shirjang S, Baradaran B. The different mechanisms of cancer drug resistance: a brief review. *Adv. Pharm. Bull.* 7(3), 339–348 (2017).
6. Liang M, Fan K, Zhou M *et al.* H-ferritin-nanocaged doxorubicin nanoparticles specifically target and kill tumors with a single-dose injection. *Proc. Natl Acad. Sci. USA* 111(41), 14900–14905 (2014).
7. Cai X, Luo Y, Zhang W, Du D, Lin Y. pH-sensitive ZnO quantum dots-doxorubicin nanoparticles for lung cancer targeted drug delivery. *ACS Appl. Mater. Interfaces* 8(34), 22442–22450 (2016).
8. Tang X, Loc WS, Dong C *et al.* The use of nanoparticulates to treat breast cancer. *Nanomedicine* 12(19), 2367–2388 (2017).
9. Barenholz Y. Doxil®–the first FDA-approved nano-drug: lessons learned. *J. Control. Rel.* 160(2), 117–134 (2012).
10. Shafiei M, Ansari MNM, Razak SIA, Khan MUA. A comprehensive review on the applications of exosomes and liposomes in regenerative medicine and tissue engineering. *Polymers (Basel)* 13(15), 2529 (2021).
11. Tian Y, Li S, Song J *et al.* A doxorubicin delivery platform using engineered natural membrane vesicle exosomes for targeted tumor therapy. *Biomaterials* 35(7), 2383–2390 (2014).
12. Ohno S, Takanashi M, Sudo K *et al.* Systemically injected exosomes targeted to EGFR deliver antitumor microRNA to breast cancer cells. *Mol. Ther.* 21(1), 185–191 (2013).
13. Sugahara KN, Teesalu T, Karmali PP *et al.* Tissue-penetrating delivery of compounds and nanoparticles into tumors. *Cancer Cell* 16(6), 510–520 (2009).
14. Timur SS, Yalçın G, Çevik Ö, Andaç C, Gürsoy RN. Molecular dynamics, thermodynamic, and mutational binding studies for tumor-specific LyP-1 in complex with p32. *J. Biomol. Struct. Dyn.* 36(5), 1134–1144 (2018).
15. Roth L, Agemy L, Kotamraju VR *et al.* Transtumoral targeting enabled by a novel neuropilin-binding peptide. *Oncogene* 31(33), 3754–3763 (2012).
16. Vivian J, Rao AA, Nothaft FA *et al.* Toil enables reproducible, open source, big biomedical data analyses. *Nat. Biotechnol.* 35(4), 314–316 (2017).
17. Goldman MJ, Craft B, Hastie M *et al.* Visualizing and interpreting cancer genomics data via the Xena platform. *Nat. Biotechnol.* 38(6), 675–678 (2020).
18. Győrffy B. Survival analysis across the entire transcriptome identifies biomarkers with the highest prognostic power in breast cancer. *Comput. Struct. Biotechnol. J.* 19, 4101–4109 (2021).
19. Li Q, Birkbak NJ, Gyorffy B, Szallasi Z, Eklund AC. Jetset: selecting the optimal microarray probe set to represent a gene. *BMC Bioinformatics* 12, 474–480 (2011).
20. Hung ME, Leonard JN. Stabilization of exosome-targeting peptides via engineered glycosylation. *J. Biol. Chem.* 290(13), 8166–8172 (2015).
21. Berry MG, Gui GP, Wells CA, Carpenter R. Integrin expression and survival in human breast cancer. *Eur. J. Surg. Oncol.* 30(5), 484–489 (2004).
22. Chen YB, Jiang CT, Zhang GQ, Wang JS, Pang D. Increased expression of hyaluronic acid binding protein 1 is correlated with poor prognosis in patients with breast cancer. *J. Surg. Oncol.* 100(5), 382–386 (2009).
23. Wang J, Song Y, Liu T *et al.* Elevated expression of *HABP1* is a novel prognostic indicator in triple-negative breast cancers. *Tumour Biol.* 36(6), 4793–4799 (2015).
24. Bai J, Duan J, Liu R *et al.* Engineered targeting tLyp-1 exosomes as gene therapy vectors for efficient delivery of siRNA into lung cancer cells. *Asian J. Pharm. Sci.* 15(4), 461–471 (2020).
- **Similar engineering design for exosomes as the current study.**
25. Tsai SJ, Atai NA, Cacciottolo M *et al.* Exosome-mediated mRNA delivery *in vivo* is safe and can be used to induce SARS-CoV-2 immunity. *J. Biol. Chem.* 297(5), 101266 (2021).
26. Fordjour FK, Guo C, Ai Y, Daaboul GG, Gould SJ. A shared stochastic pathway mediates exosome protein budding along plasma and endosome membranes. *J. Biol. Chem.* 298(10), 102394 (2022).
27. Lin D, Zhang H, Liu R *et al.* iRGD-modified exosomes effectively deliver CPT1A siRNA to colon cancer cells, reversing oxaliplatin resistance by regulating fatty acid oxidation. *Mol. Oncol.* 15(12), 3430–3446 (2021).
- **Similar engineering design for exosomes as the current study.**
28. Liu Q, Dai G, Wu Y *et al.* iRGD-modified exosomes-delivered BCL6 siRNA inhibit the progression of diffuse large B-cell lymphoma. *Front. Oncol.* 12, 822805 (2022).
- **Similar engineering design for exosomes as the current study.**
29. Wei H, Chen J, Wang S *et al.* A nanodrug consisting of doxorubicin and exosome derived from mesenchymal stem cells for osteosarcoma treatment *in vitro*. *Int. J. Nanomed.* 14, 8603–8610 (2019).
30. Lennaárd AJ, Mamand DR, Wiklander RJ, El Andaloussi S, Wiklander OPB. Optimised electroporation for loading of extracellular vesicles with doxorubicin. *Pharmaceutics* 14(1), 38 (2021).

31. Thakur A, Sidu RK, Zou H, Alam MK, Yang M, Lee Y. Inhibition of glioma cells' proliferation by doxorubicin-loaded exosomes via microfluidics. *Int. J. Nanomed.* 15, 8331–8343 (2020).

32. Gomari H, Forouzandeh Moghadam M, Soleimani M. Targeted cancer therapy using engineered exosome as a natural drug delivery vehicle. *OncoTargets Ther.* 11, 5753–5762 (2018).

33. Chen C, Sun M, Wang J, Su L, Lin J, Yan X. Active cargo loading into extracellular vesicles: highlights the heterogeneous encapsulation behaviour. *J. Extracell. Vesicles* 10(13), e12163 (2021).

34. Sebaugh JL. Guidelines for accurate EC_{50}/IC_{50} estimation. *Pharm. Stat.* 10(2), 128–134 (2011).

35. Schindler C, Collinson A, Matthews C *et al.* Exosomal delivery of doxorubicin enables rapid cell entry and enhanced *in vitro* potency. *PLOS ONE* 14(3), e0214545 (2019).